

# Design and Development of a High-Frequency Multiport Solid-State Transformer With Decoupled Control Scheme

Mohammad Rashidi , Necmi N. Altin , Senior Member, IEEE, Saban S. Ozdemir , Member, IEEE, Abedalsalam Bani-Ahmed, Member, IEEE, and Adel Nasiri , Senior Member, IEEE

**Abstract**—In this article, a four-port solid-state transformer and a control scheme to control the power flow and output voltage are studied, developed, and tested. The converter consists of three ports with H-bridge converters and one port with a diode bridge rectifier. The ports with H-bridge converters are capable of bidirectional power routing as well as reactive power contribution in a volt/Var control scenario. The diode bridge rectifier provides a dc voltage for load connection. Different arrangements for the four transformer windings are analyzed, simulated, and compared to achieve an optimal design. A new control strategy, which uses a combination of phase-shift and duty cycle control, is employed to control the flow of power between the converter branches and to regulate the output voltage. While phase-shift control ensures the balance of power on each port based on a reference value, the duty cycle control keeps the load voltage at a desired voltage level. A high-level control scheme is employed to determine the power references for all ports according to the load demand, generation capacity of the distributed generation system, and state of charge of the energy storage. The performance of the proposed system is validated with simulation and experimental analysis. A prototype is designed and built with 10-kW power rating at each port. The operating frequency of the system is designed at 100 kHz to obtain a very compact size for the whole converter.

**Index Terms**—Duty cycle control, high frequency, multiport transformer, phase-shift control, solid-state transformer (SST).

Manuscript received January 2, 2019; revised April 30, 2019 and July 16, 2019; accepted August 1, 2019. Date of publication September 4, 2019; date of current version November 7, 2019. Paper 2018-HPC-1426.R2, approved for publication in the IEEE TRANSACTIONS ON INDUSTRY APPLICATIONS. This work was supported by the National Science Foundation under Grant 1650470. The work of N. Altin and S. Ozdemir was supported by the Scientific and Technological Research Council of Turkey (TUBITAK) BIDEB-2219 Postdoctoral Research program. (Corresponding author: Adel Nasiri.)

M. Rashidi and A. Bani-Ahmed are with Eaton Research Labs—Eaton, Menomonee Falls, WI 53051 USA (e-mail: morashidi@eaton.com; salamabaniahmed@eaton.com).

N. N. Altin is with the Center for Sustainable Electrical Energy Systems, University of Wisconsin-Milwaukee, Milwaukee, WI 53211 USA, and also with the Department of Electrical & Electronic Engineering, Faculty of Technology, Gazi University, Ankara 06560, Turkey (e-mail: altin@uwm.edu).

S. S. Ozdemir is with the Center for Sustainable Electrical Energy Systems, University of Wisconsin-Milwaukee, Milwaukee, WI 53211 USA, and also with the Department of Energy Systems Engineering, Faculty of Technology, Gazi University, Ankara 06560, Turkey (e-mail: ozdemir@uwm.edu).

A. Nasiri is with the Electrical Engineering and Computer Science Department at the University of Wisconsin-Milwaukee, Milwaukee, WI 53211 USA (e-mail: nasiri@uwm.edu).

Color versions of one or more of the figures in this article are available online at <http://ieeexplore.ieee.org>.

Digital Object Identifier 10.1109/TIA.2019.2939741

## I. INTRODUCTION

THE concept of solid-state transformer (SST) in different forms has been studied in several articles since early 1980s [1]–[6]. SST is a combination of power electronics (PE) converters and a high frequency transformer which is used to connect isolated voltage zones. In addition to the normal functionalities of the conventional transformers [7] such as galvanic isolation and voltage matching, a PE-based transformer benefits the power distribution system by enabling active power and voltage control, and real-time monitoring and control of the connected elements. Besides, the high-frequency operation of the transformer makes the total size of the SST much smaller than a conventional low frequency transformer with the same voltage and power ratings. There are two major factors driving further advancement in SST technology; the growing need for the compact and controllable converters to integrate more distributed energy resources, and the recent developments of high-power and high-frequency PEs switches which allow efficient operation of switches at higher frequency [8].

The study in [9] is focused on the local installation of energy storage as one of the main requirements for the future architecture of the distribution system for supporting local demands. When photovoltaic systems, battery units and/or fuel cells are employed, several two-port dc–dc converters are adopted to control and manage the system. This need for multiple PE converters decreases the power density and reliability [10]. The SSTs in this system provide voltage matching, and galvanic isolation with improved power density. However, the need for multiple dc–dc converters affects the power density and reliability factor negatively. Multiport converters are good options to tackle this problem in the systems with multiple converters. Isolated multiport converters can be categorized in two groups. In the first group, the converter is designed to connect higher number of sources than the number of windings to a transformer [11], [12]. In the system with multiple sources on one winding, the number of windings and total number of power switches are reduced, but some of the ports share a common ground and complete galvanic isolation cannot be obtained. In addition, the connection of the different voltage levels on the same winding using one level PE converter is difficult. The second category has a transformer with one winding for each port. In this topology, all of the components are galvanically isolated from each

other and the transformer turn ratio can be used to adjust the voltage level between different connected elements. The SST concept which includes HF transformer and minimizes the size of the transformer is a proper option for the second category of multiport converters to keep the size and weight of the converter optimized.

The SST-based multiport converters have been discussed and used for different applications including traction (electrical trains) [13]–[16], electrical vehicle power distribution systems [11], [17], [18], hybrid distributed generation (DG), and dc power distribution applications [10], [19]–[22]. In [10], [11], and [17], three-port dc–dc converter topology and some control schemes for this topology are proposed and illustrated. The concept of three-port SST which enables having a dc port for direct integration of energy storage systems (ESS) into the power network is described in [23]. In [19], an SST topology is introduced based on a quad-active bridge (QAB) topology for utilizing DG in the grid. All of the ports of the QAB are connected to active switch-based converters.

It is possible to have converters with higher number of ports, but control and magnetic design complexity limits the number of ports. The multiport converters presented in [13] and [15] have many primary windings and two secondary windings which are connected to two separate traction motors. The voltage on one side of this converter is medium voltage and several primary windings are used to interface with the medium-voltage grid. The power flow is bidirectional between primary and secondary. However, there is no power flow among the primary windings, or among the secondary windings.

Multiport SST (MSST) or multiport isolated converter topology is an extension version of the dual-active bridge (DAB) converters. Generally, in the DAB converters, the flow of power from one port to another is controlled by the phase-shift angle between these two ports. Several studies have focused on three-port SST applications [11], [24], [25] which is an extended version of DAB. Later, four-port systems have been introduced [19]. The phase-shift control in different forms is still the common method to control the power exchange of the ports and output voltage regulation [10], [17], [19], [22] and [26] for the DAB and QAB converters. In the QAB system, the higher phase-shift value in some operation modes causes high reactive power and circulating current. Also, under the low-load conditions, this method results in relatively high current [27]. Therefore, in some studies, the duty cycle control is applied along with the phase-shift control to improve the system control [11], [17], [25]. The duty cycle control in these studies is applied to regulate the supply voltage variations. If the battery or ultracapacitor is connected to the system, the dc voltage varies with power fluctuations. In this case, the converter that is connected to this port acts as a buck–boost converter and the duty cycle of the converter is controlled to regulate this variation. The duty cycle control is applied in [13] to regulate the power flow and/or output voltage. The studied system has many primary and secondary windings, but the power flow is always unidirectional.

In this article, a four-port SST topology is developed to be used as a compact integration node for several voltage zones such as DG, ESS, grid and load in a distribution system. Fig. 1

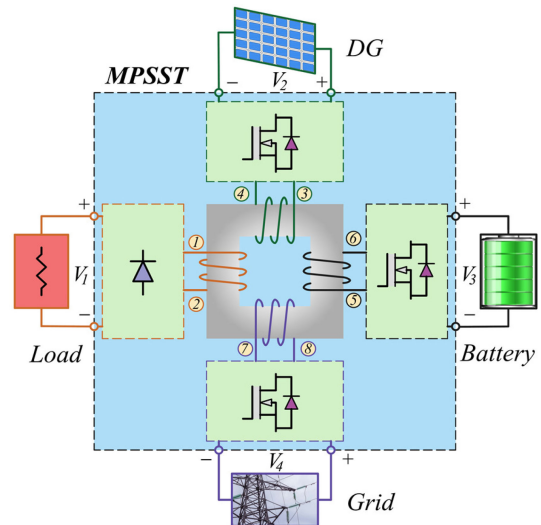


Fig. 1. Configuration of the proposed MPSST connecting two ac systems, an ESS, and a DG.

shows the four-port topology of the proposed MPSST of this study.

Three of the ports of this MPSST include an active converter for integration of the grid, the ESS and the DG source in the system. The full-bridge single-phase converters are used as active converters for these ports. Due to the nongenerating nature of the load, a unidirectional single-phase diode bridge rectifier is used in the load port. For the application in the ac system, each of these ports needs to be connected to a low frequency single or three-phase inverter. A decoupled power control model is proposed, and both phase-shift control and duty cycle control methods are employed to control the power flow from different ports and the load voltage. A power management method is developed to determine the share of power of each port in different operating modes. This method determines the power references for the ports, and the active converters are controlled to meet these reference signals. The operation of the proposed system is validated with MATLAB/Simulink simulation and experimental tests which are performed on a 10 kW/port MPSST prototype.

## II. PROPOSED FOUR-PORT SST

### A. Four-Port Transformer Design

The high-frequency transformer is the main element of the SST configuration. To have the best performance from the HF transformer, optimal material and geometry selection of the core, winding wires are very important. Also, for the case of the multiwinding transformer of this study, the winding placement is a significant factor to achieve efficient controllable flux flow and better coupling coefficient between the windings.

The efficient operation of the transformer is directly affected by the design of the transformer core and selection of the core material. For a practical core material selection, four parameters including flux density, price and availability, optimal frequency

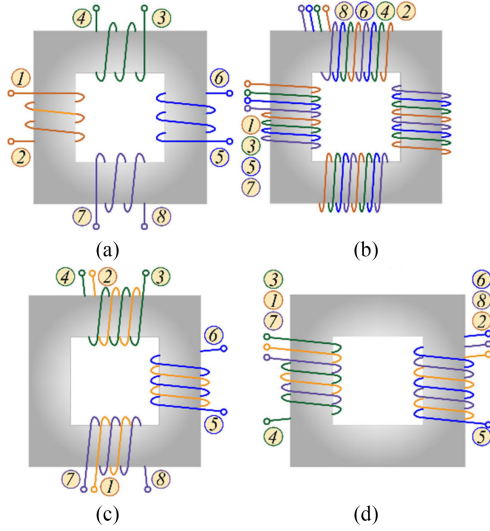


Fig. 2. Test cases of MPSST windings placement. (a) Case A. (b) Case B. (c) Case C. (d) Case D ((1–2) represents load port (orange), (3–4) represents DG port (green), (5–6) represents ESS port (blue), and (7–8) represents grid port (purple).)

range, and core losses are considered. Silicon steel, ferrite, amorphous and nanocrystalline are studied as the core material options for this transformer. The operating frequency is determined considering various factors including, power density, switching losses, and core losses and copper (winding) losses. There are some studies about the relation between the operating frequency and these losses [28]–[31]. Based on these parameters, the maximum operating frequency of the converter is determined to be 100 kHz. Ferrite is the selected material for the core of this transformer. Although the flux density of the ferrite is smaller ( $<0.4$  T) than the other materials, it has the best power loss characteristics at higher frequency operations. Also, ferrite is easily available in the market in different sizes and lower prices.

A minimum level of leakage inductance is required to obtain power flow and limit the winding current. However, large leakage inductance value also limits the power transfer capability of the system. Therefore, the placement of the four windings of the transformer is also investigated. The winding placement affects the leakage inductance, winding to winding capacitance, coupling factor between the windings, and the length of the wire. Four of the possible winding placement options are considered and simulated in ANSYS/Maxwell 3D software to calculate the coupling factors for different cases. The winding placement cases are shown in Fig. 2. The simulation results for these four possible options are given in Table I. The winding placement of Cases B and C provide the best coupling coefficients for feeding the fourth winding. However, Case B uses more wires for the windings which increases the wire resistance and affects the efficiency negatively. Thus, Case C is selected as winding placement for the proposed four-port transformer design. The obtained flux distribution from simulation studies is given in Fig. 3. As it is shown from the figure, no significant saturation occurs at the worst case of the frequency (100 kHz).

TABLE I  
COUPLING COEFFICIENT FOR DIFFERENT WINDING PLACEMENTS

Case A	W1	W2	W3	W4
W1	1.00	0.93	0.94	0.94
W2	0.93	1.00	0.94	0.94
W3	0.94	0.94	1.00	0.92
W4	0.94	0.94	0.92	1.00
Case B	W1	W2	W3	W4
W1	1.00	0.99	0.99	0.99
W2	0.99	1.00	0.99	0.99
W3	0.99	0.99	1.00	0.99
W4	0.99	0.99	0.99	1.00
Case C	W1	W2	W3	W4
W1	1	0.92	0.93	0.97
W2	0.92	1	0.93	0.97
W3	0.93	0.93	1	0.97
W4	0.97	0.97	0.97	1
Case D	W1	W2	W3	W4
W1	1	0.93	0.97	0.97
W2	0.93	1	0.97	0.97
W3	0.97	0.97	1	0.97
W4	0.97	0.97	0.970	1

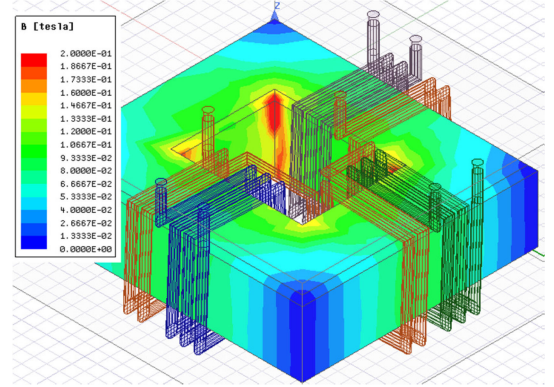


Fig. 3. Flux distribution of the proposed four-port transformer.

### B. Four-Port Converter and Control Design

The control of the four-port SST is based on the same equations as the control of a DAB converter. Therefore, the equation for delivered power from port- $x$  to port- $y$  is written as follows [2]:

$$P_{xy} = \frac{V'_x V'_y}{2\pi^2 f_s L_{xy}} \phi_{xy} (\pi - \phi_{xy}) \quad \phi_{xy} = \phi_x - \phi_y \quad (1)$$

where  $P_{xy}$  is the power (W) transferred from port- $x$  to port- $y$ ;  $\phi_x$  and  $\phi_y$  are phase-shift angles (radian) of the converters connected to port- $x$  and port- $y$ , respectively;  $V'_x$  and  $V'_y$  are dc voltages (V) referred to the ac side of port- $x$  and port- $y$ , respectively;  $f_s$  is the switching frequency (Hz) and  $L_{xy}$  is the equivalent inductance (H) between the port- $x$  and port- $y$ .

In this study, a four-port SST is proposed as depicted in Fig. 4. Here,  $L_1$ ,  $L_2$ ,  $L_3$ , and  $L_4$  are the corresponding winding leakage inductances combined with external inductors. For simplicity, mutual-leakage inductances presented in [24] are not considered here. The power flow between any two ports is calculated by (1). The equivalent circuit given in Fig. 5 can be obtained from Fig. 4. Here,  $L_m$  is the magnetizing inductance;  $L_1$  is the leakage

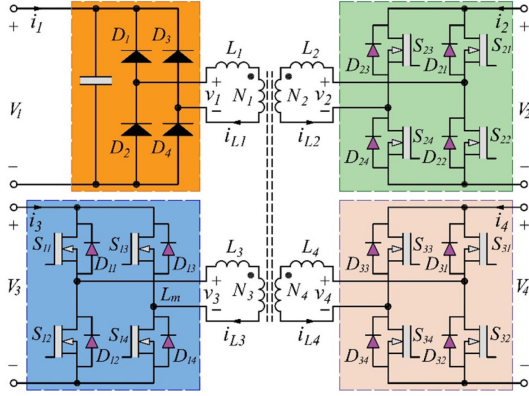


Fig. 4. Circuit configuration of the four-port SST.

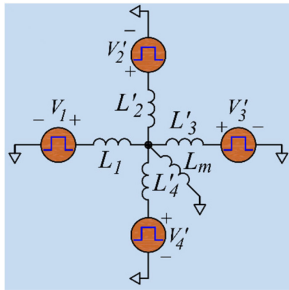


Fig. 5. Equivalent circuit of the four-port SST.

inductance of port-1; and  $L'_2$ ,  $L'_3$ , and  $L'_4$  are leakage inductances of Ports 2–4 referred to the side of port-1;  $v_1$ ,  $v'_2$ ,  $v'_3$ ,  $v'_4$  and  $i_1$ ,  $i'_2$ ,  $i'_3$ ,  $i'_4$  are port voltages and currents referred to the port-1. It is clear from Fig. 5 and (1) that the equivalent inductances between the ports should be obtained to calculate the power flow. Thevenin equivalent circuit can be used for this purpose. The Thevenin equivalent circuit between the port- $x$  and port- $y$  referred to port-1 is given in Fig. 6(a) [19]. Equations for the equivalent inductances are given in the Appendix.

Similarly, the Thevenin-equivalent voltages can be written for this circuitry. However, the Thevenin-equivalent voltage of a port is not the same for every power flow analysis. For instance, the Thevenin-equivalent voltage of port-3 is written in (2) and (3) when power flows from port-1 to port-3 and from port-2 to port-3, respectively

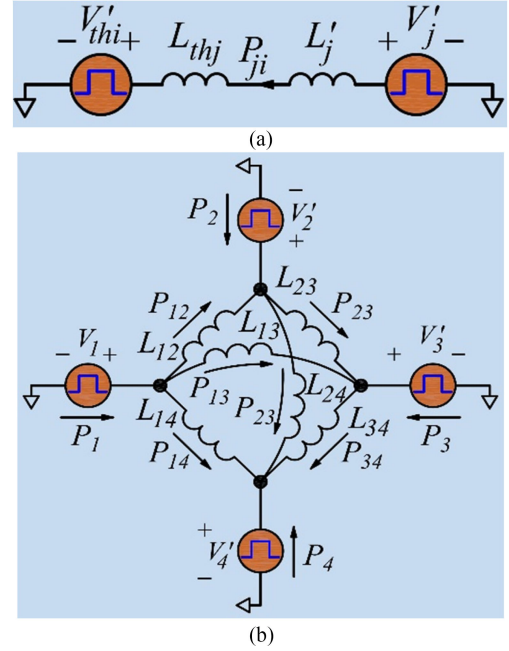
$$v_{\text{TH3-3}} = \frac{L'_2 L'_4}{L'_2 L'_3 + L'_2 L'_4 + L'_3 L'_4} v'_3 \quad (2)$$

$$v_{\text{TH3-2}} = \frac{L'_1 L'_4}{L'_1 L'_3 + L'_1 L'_4 + L'_3 L'_4} v'_3. \quad (3)$$

After obtaining all of the equivalent inductances between the ports, the equivalent circuit, which is used to calculate the flowing power between the ports and total port power, is calculated and shown as in Fig. 6(b). According to the current directions, the power equations for each port can be written as follows:

$$P_2 = P_{12} - P_{23} - P_{24} \quad (4)$$

$$P_3 = P_{13} + P_{23} - P_{34} \quad (5)$$

Fig. 6. (a) Thevenin equivalent circuit between the port- $x$  and port- $y$  referred to port- $x$ . (b) Equivalent circuit representing equivalent inductances among the ports.

$$P_4 = P_{14} + P_{24} + P_{34} \quad (6)$$

$$P_1 = -P_2 - P_3 - P_4. \quad (7)$$

Then, using (1) and (4)–(7), power equations for each port can be obtained. The obtained power equations are given in the Appendix. It can be seen from equations that the power of each port depends on all of the three phase angles. This makes the control of the system very complicated. Therefore, a small gain ( $x + \Delta x$ ) linearization method is applied to the power equations to decouple the equations. Then, power equations have steady-state and perturbation variables as  $P_x$ ,  $\phi_x$ ,  $\Delta P_x$ , and  $\Delta \phi_x$  [32]. These  $\Delta \phi_x$  perturbation control variables can be used in control loop to control the power flow, and power variation components can be written in the linear system equation form as follows:

$$\Delta P = K \cdot \Delta \phi \quad (8)$$

$$\begin{bmatrix} \Delta P_2 \\ \Delta P_3 \\ \Delta P_4 \end{bmatrix} = \begin{bmatrix} (a + b + c) & -b & -c \\ -b & (b + d + e) & -e \\ -c & -e & (c + e + f) \end{bmatrix} \begin{bmatrix} \Delta \phi_2 \\ \Delta \phi_3 \\ \Delta \phi_4 \end{bmatrix} \quad (9)$$

where  $a = \frac{V_1 V_{\text{TH2-2}}}{2\pi^2 f_s L_{12}} (-2\phi_2 + \pi)$ ,  $b = \frac{V_2 V_{\text{TH3-3}}}{2\pi^2 f_s L_{23}} (-2\phi_3 + 2\phi_2 + \pi)$ ,  $c = \frac{V_2 V_{\text{TH4-4}}}{2\pi^2 f_s L_{24}} (-2\phi_4 + 2\phi_2 + \pi)$ ,  $d = \frac{V_1 V_{\text{TH3-3}}}{2\pi^2 f_s L_{13}} (-2\phi_3 + \pi)$ ,  $e = \frac{V_3 V_{\text{TH4-4}}}{2\pi^2 f_s L_{34}} (-2\phi_3 + 2\phi_2 + \pi)$ , and  $f = \frac{V_1 V_{\text{TH4-4}}}{2\pi^2 f_s L_{14}} (-2\phi_4 + \pi)$ . The control variable can be calculated depending on the required power variations in accordance to

$$\Delta \phi = K^{-1} \cdot \Delta P. \quad (10)$$

TABLE II  
PPM MODES OF OPERATION FOR THE MPSST CONVERTER

Constraints	Power Sharing
1 $ P_{DG}  \geq  P_{Load}$ $SoC \geq 0.95$	$ P_G  =  P_{DG}  -  P_L $ $ P_{ES}  = 0$
2 $ P_L  <  P_{DG}  \leq  P_L  + (0.95 - SoC) * B_{cap}$ $SoC < 0.95$	$ P_G  = 0$ $ P_{ES}  =  P_{DG}  -  P_L $
3 $ P_L  + (0.95 - SoC) * B_{cap} \leq  P_{DG} $ $SoC \leq 0.95$	$ P_{ES}  = (0.95 - SoC) * B_{cap}$ $ P_G  =  P_{DG}  -  P_L  -  P_{ES} $
4 $ P_L  =  P_{DG} $	$ P_G  = 0$ $ P_{ES}  = 0$
5 $ P_{DG}  <  P_L  \leq  P_{DG}  + (SoC - 0.2) * B_{cap}$ $SoC > 0.2$	$ P_G  = 0$ $ P_{ES}  =  P_L  -  P_{DG} $
6 $ P_{DG}  + (SoC - 0.2) * B_{cap} <  P_L $ $SoC > 0.2$	$ P_{ES}  = (SoC - 0.2) * B_{cap}$ $ P_G  =  P_L  -  P_{DG}  -  P_{ES} $
7 $ P_{DG}  <  P_L $ $SoC \leq 0.2$	$ P_{ES}  = 0$ $ P_G  =  P_L  -  P_{DG} $

As it is shown in (10), the power variation of any port is dependent on only its control variable, and thus decoupled power flow control is obtained.

### III. SYSTEM POWER AND VOLTAGE CONTROL

#### A. Power Sharing Control Strategy

The phase-shift control method controls the power flow between the ports. The power reference for each port should be determined to sustain the operation of the system. Thus, the first layer of the system control consists of a power sharing control logic which generates the current reference for each leg based on the parameters of the sources. Different constraints and priorities can be defined and based on them different power sharing control algorithms can be designed for this purpose. In this study, the proposed algorithm is called the pool of power method (PPM). PPM uses the state of charge (SoC) of the ESS, power generation capacity of the DG port, and the load demand as inputs of the decision-making chart, and calculates the power reference of the of the different ports as expressed in

$$[P_G, P_{ES}] = f(SoC, P_{DG}, P_L). \quad (11)$$

Assuming the grid connection port is always available with at least the capacity equal to the maximum of the load, the system is planned to always supply the load power demand and absorb all of the generated power of the DG. The outputs of the PPM chart are the exchanged (positive or negative) power of the grid and energy storage ports. This chart is continuously running during the operation of the system, as the DG power and SoC of the energy storage are changing during the operation. Various power sharing scenarios for the converter are given in Table II. Seven possible modes of operations are defined for the power sharing of the proposed four-port SST topology. Beside the main constraints of meeting the load demand, the extra generated power of the DG port is stored by energy storage or exported to the grid in some operation modes. The priority chart of Table II is the decision-making process to determine the demanded share of power at each port. Ultimately, the load demand should be

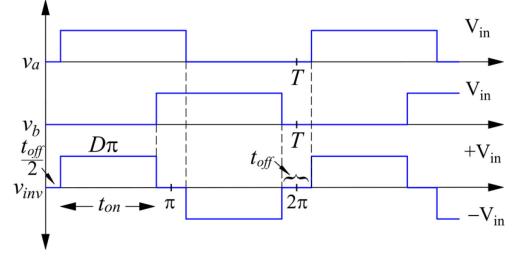


Fig. 7. Output voltage of each active H-bridge converter.

equal to the summation of the power provided from the other ports of the converter.

#### B. Duty Cycle Control

The proposed four-port SST topology employs three high frequency H-bridge inverters on the three active ports and one diode rectifier on the load port. Although the power balance between the source ports and load port is ensured and output voltage can be kept constant at its desired level by controlling the phase-shift angles of the three ports, especially under the low load condition, increasing the phase shift increases the reactive power and RMS value of the current [27]. This reactive power does not support the active power flow, but it circulates through the leakage inductances and MOSFETs and/or antiparallel diodes (depending on the switching state and current polarity). The converter suffers from high circulating current and its efficiency deteriorates. Therefore, besides the phase-shift control, the duty cycle control is presented for controlling this converter. By adding a phase shift between the legs of the converters on the active ports, duty cycles and effective values of the voltages applied to the transformer windings are controlled as shown in Fig. 7. The ac side waveform of each converter is a repeating square wave voltage. Equation (12) defines this voltage

$$V_i = \begin{cases} 1 & 0 \leq t < t_{on} \\ 0 & t_{on} \leq t < \frac{T}{2} \\ -1 & \frac{T}{2} \leq t < \frac{T}{2} + t_{on} \\ 0 & \frac{T}{2} + t_{on} \leq t < T \end{cases} \quad (12)$$

Here, the ratio between the  $t_{on}$  and  $T$  in Fig. 7 is the duty cycle ( $D$ ) of the waveform. The general Fourier transform for this waveform including the phase shift is described by

$$V_i(t) = \sum_{n=1}^{\infty} (a_{ni} \cos(n\omega_0 t)) \quad (13)$$

$$a_{ni} = 2 \cdot \frac{2V_{DCi}}{n\pi} \sin\left(n\pi \frac{t_{oni}}{T}\right). \quad (14)$$

These equations show that the harmonic content of the waveform changes by changing the duty cycle of the square-wave voltage. The RMS value of this voltage is described in

$$V_{RMSsquare} = V_{PSquare} \sqrt{2D}. \quad (15)$$

Since the duty cycle control changes the harmonic content and RMS value of the output voltage of each inverter, it will

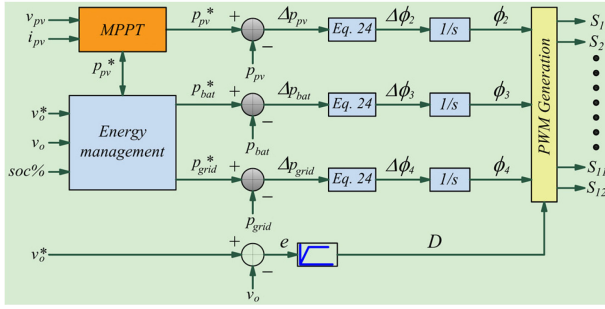


Fig. 8. Block diagram of the proposed decoupled controller.

ultimately affect the voltage regulation. This capability expands the range of power adjustment of the controller. The proposed control of this study includes an outer control loop which adjusts the duty cycle for different load situation. Then, the decoupled phase-shift control will enforce the expected share of power of each port as well as voltage and power regulation at the load port. The complete control block diagram that employs phase-shift control and duty cycle control is shown in Fig. 8.

### C. Dynamic Analysis

The proposed system has four ports which includes a load port, a DG port that provides unidirectional power flow, a bidirectional port for the grid, and ESS ports. Since there are four control parameters (three-phase shift angles and a duty cycle value), modeling and analyzing the system with traditional methods are not straightforward. Therefore, in this study, dynamic performance of the system is investigated with a numerical model. Since there are four ports, and the operation conditions of the system are dependent on DG source, ESS and/or grid conditions, a test scenario is selected to make a dynamic analysis. In this scenario, the power levels of the DG and grid ports are considered as constant. Then, an abrupt load change is applied to the load port and dynamic performance of the proposed system and the control scheme is investigated. The system control block diagram for this condition is depicted in Fig. 9(a). The control blocks for the DG port and grid port are not depicted in the figure. However, since the phase-shift angle values of these two ports affect the power level of the ESS port, they have to be considered, and thus they are shown in the figure. The phase-shift angles and power levels for these two ports are calculated using (10), (15) and (22)–(24).

The dynamic response of the proposed four-port transformer and decoupled control scheme with duty cycle control is shown in Fig. 9(b). Here, the input voltage for the three ports is constant at 200 V, and the output voltage reference is 400 V. The gains of the PI controllers are  $K_{p1} = 500$ ,  $K_{i1} = 12500$ ,  $K_{p2} = 1000$ ,  $K_{i2} = 15000$ . It is seen that the proposed system has fast dynamic response. Since the load-side capacitor is not considered in the model, there is an instant decrease on voltage. However, the proposed method can recover it very fast. In addition, the performance of the decoupled control is also shown in the figure. When the load changes, the required power is provided by Port 3 (ESS port) and the power levels of Port 2 (DG port) and Port 4

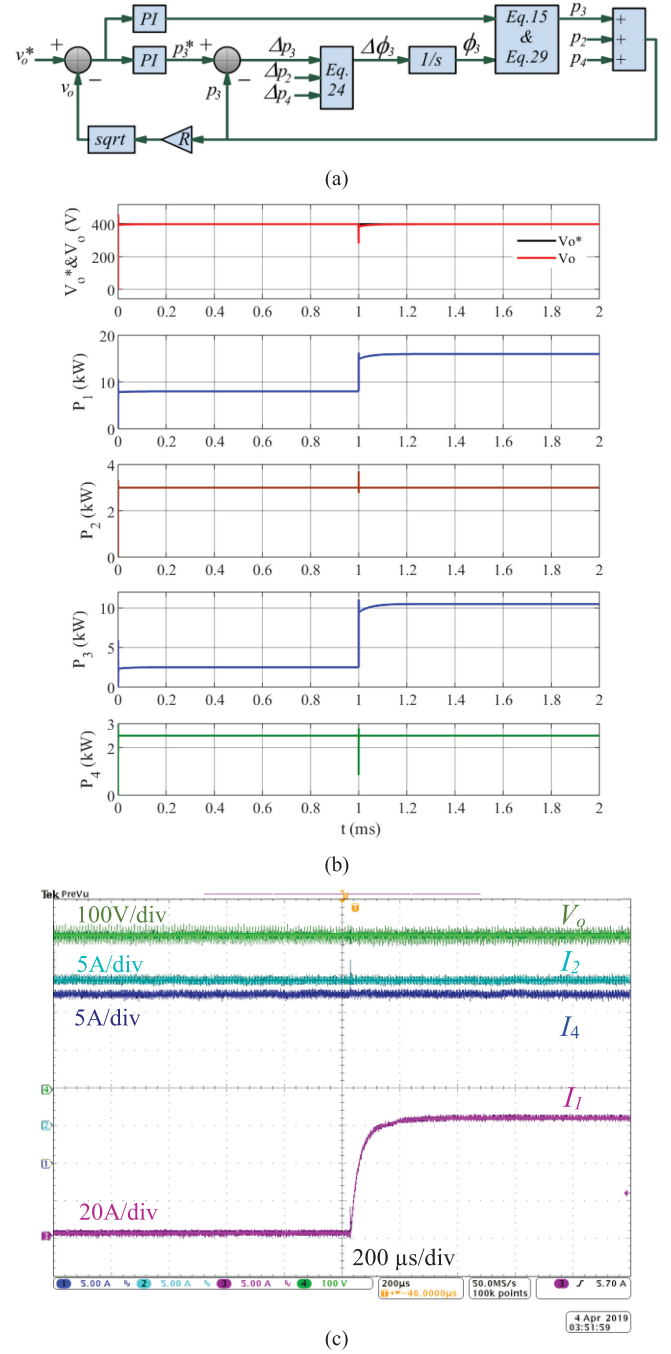


Fig. 9. (a) Control block diagram used for dynamic analysis for given test scenario. (b) Simulation results of the dynamic response of the proposed system for given test scenario. (c) Experimental results of the dynamic response of the proposed system for given test scenario (Ch.1 is the grid current (5 A/div), Ch. 2 is the DG current (5 A/div), Ch. 3 is the load current (5 A/div), and Ch. 4 is the load voltage (100 V/div)).

(Grid Port) are kept constant by controlling only duty cycle and the phase shift of each port. The same scenario is tested with experimental setup. Again, the DG power and grid power references are kept constant, and step load change is applied to the load port. The output voltage (Ch. 4), the grid port current (Ch. 1), DG port current (Ch. 2), and load current (Ch. 3) are

TABLE III  
SYSTEM PARAMETERS

Characteristic	Value
Input Voltages	200-400V
Passive Port Output Voltage	Load leg 400V
Nominal Power	Each port-10kW
Target Frequency	100kHz
Transformer Core Material	Ferrite, B: 0.25T
Transformer Winding Wire	Litz Wire, Eq 8AWG- 38AWG strand
Leakage and Magnetizing Inductance	$L_{\lambda(1-j)} = 2\mu\text{H}$ ; $L_m = 75\mu\text{H}$
Chosen Switch Modules	SiC MOSFET module
Fast Recovery Diode Modules	IXYS DSEI 2x 61-10B X2
DC Bus Capacitors	68 $\mu\text{F}$



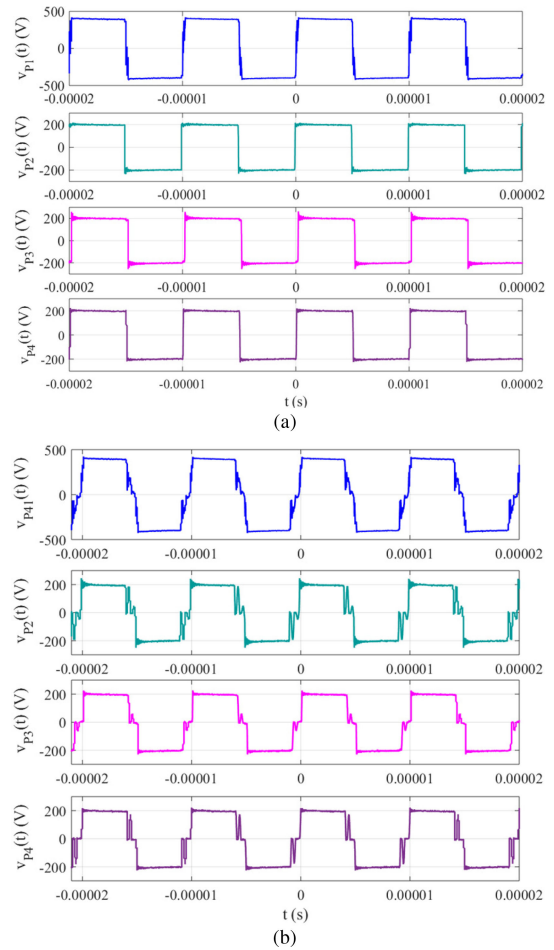
Fig. 10. Implemented 10 kW/port MPSST in the lab.

given in Fig. 9(c). Since the DG power reference and grid power reference are balanced, the required power is provided by the ESS port. It is seen from the figure that the proposed system is stable and provides fast dynamic response.

#### IV. SIMULATION AND EXPERIMENTAL VALIDATIONS

The proposed four-port SST and the control scheme is validated using simulation and experimental results. The simulation is performed in MATLAB/Simulink environment. The control scheme is implemented on Altera field-programmable gate array board. The switching frequency is 100 kHz for all of the four ports. The system parameters used in the transformer design, simulation and experimental studies are given in Table III. The hardware setup is shown in Fig. 10. The voltage value of the input ports is 200 V and kept constant, and the reference value for the output voltage is 400 V.

It is assumed in the proposed system that one port is connected to the DG source, the second port is connected to the battery ESS, next one is connected to the grid, and the last port is connected to the load. In this system, many different scenarios can be designed and implemented. Since the main purpose of the study is four-port SST and control scheme design rather than the energy management algorithm design, some simple assumptions have been done about the power references of the ports. The DG port is controlled to obtain maximum available power from the DG source. Therefore, it is assumed that a MPPT controller provides a power reference for the DG port. The power levels

Fig. 11. Transformer winding voltages obtained from experimental studies for  $0^\circ$ ,  $5^\circ$ , and  $10^\circ$  phase-shift angles. (a)  $D = 0.5$ . (b)  $D \neq 0.5$ .

of the DG and load, battery SoC level, and grid condition (it is connected or not) are important for the battery and grid power references. For simplicity of the lab test, a power reference for the battery is randomly selected and the grid power reference is generated by a PI controller to keep the output voltage constant. Thus, power references for all three ports are obtained. While the phase-shift control is responsible for the power sharing among the three non-load ports, duty cycle is applied to keep the output voltage at the desired level.

The designed MPSST is tested for different conditions with different phase shift and duty cycle values. The experimental results for the converter output voltage on the transformer windings are given in Fig. 11(a) and (b) when the  $D = 0.5$  and for  $D \neq 0.5$ , respectively. It is seen in the figures that the designed transformer fulfills the design requirements for both  $D = 0.5$  and for  $D \neq 0.5$  conditions. As it is seen in the experimental results, three inverters generate and apply square-wave voltages to the three ports of the four-port SST with the calculated phase shifts and duty cycle value. As a result, a square-wave voltage is generated at the fourth port of the transformer. When the duty cycle is less than 0.5, the zero-voltage intervals are generated on the inverter output voltages, which will affect the amount

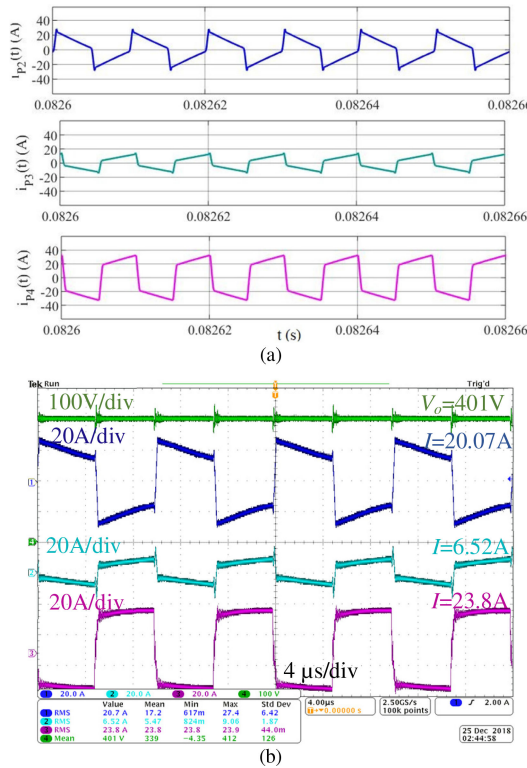


Fig. 12. Transformer winding currents for  $D = 0.5$ . (a) Simulation results. (b) Experimental results (Ch. 1 is the most leading; Ch. 3 is the most lagging port.)

of the power transferred among the windings and decrease the circulating current. In this case, the load port voltage has also zero voltage intervals, and the length of this interval can be used to control the transferred power to the load. In addition, the test results are showing that the duty cycle control does not cause any instability.

While the load power and Port 2 (Ch.1) power reference are kept constant, the power references of Port 3 (Ch. 2) and Port 4 (Ch. 3) are changed to test the performance of the four-port SST and the proposed decoupled control scheme when the duty cycle is 0.5. The transformer currents of the proposed four-port SST are given in Figs. 12 and 13.

Since the total power transferred to the load port and load resistance is constant, the output voltage stays constant. The phase-shift values define the power flow between the ports and controls the total exchanged power of each port. When the change of the reference power is applied, the proposed control scheme calculates the power error and determines the phase-shift angle for each port. Since the power reference of Port 2 (Ch. 1) is kept constant, the current of Port 2 (Ch.1) slightly changes. However, there are quiet changes on Port 3 (Ch. 2) and Port 4 (Ch. 3) currents. In both figures, Port 2 current (Ch.1) is the most leading one. While the most lagging one is Port 4 current (Ch. 3) in Fig. 12, and Port 3 current (Ch. 2) is the most lagging one in Fig. 13. The applied phase-shift values control the port currents and thus the port powers. Consequently, the power transferred to the load port is also controlled.

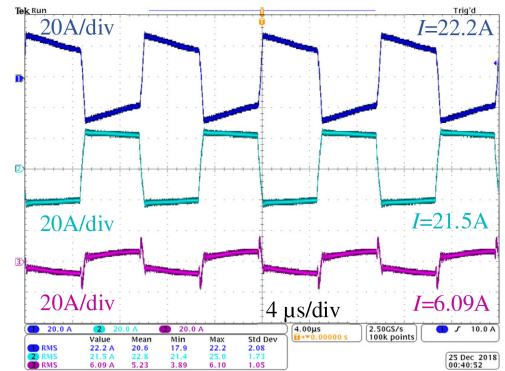


Fig. 13. Transformer winding currents for  $D = 0.5$  and higher phase-shift angles. (Ch. 1 is the most leading; Ch. 2 is the most lagging port.)

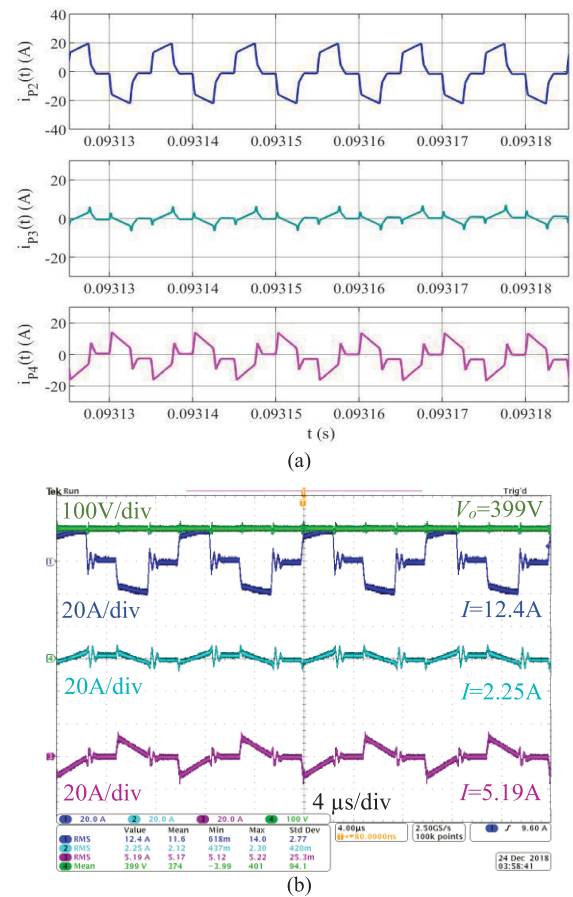


Fig. 14. Transformer winding currents for  $D \neq 0.5$ . (a) Simulation results. (b) Experimental results. (Ch. 1 is the most leading; Ch. 3 is the most lagging port.)

The duty cycle control benefits the system by increasing the degree of freedom of the system and helping to decrease the circulating current. The currents of the transformer windings of the proposed four-port SST from simulation and experimental test are given in Figs. 14 and 15. Here, while the phase-shift values are controlled to track the reference power of the ports, the duty cycle value is controlled to keep the output voltage at its desired value. In these figures, phase-shift values are almost the

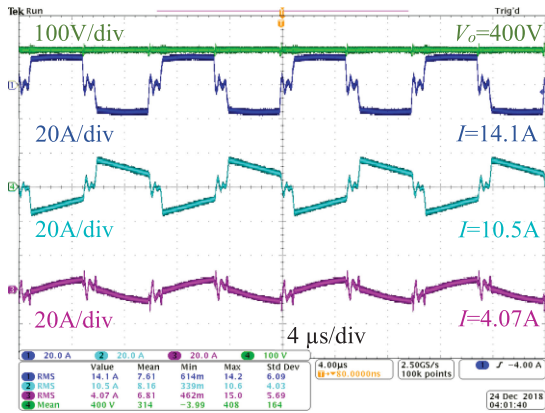


Fig. 15. Transformer winding currents for  $D \neq 0.5$ . (Ch. 1 is the most leading; Ch. 2 is the most lagging port.)

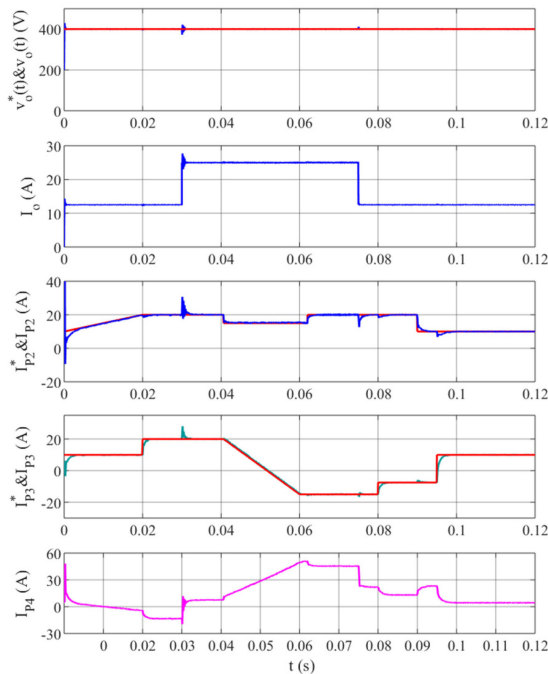


Fig. 16. Output voltage, output current, and other port currents of the proposed four-port SST for different operation conditions.

same, but while the most lagging port is Port 4 (Ch. 3) in Fig. 14, the most lagging port in Fig. 15 is Port 2 (Ch. 2). However, the duty cycle value in Fig. 14 is lower than the duty cycle in Fig. 15 due to the port power references. Under any condition, the output voltage is kept constant. It is seen that the duty cycle control does not introduce any negative effect on the system performance, and it makes the control easier and helps in decreasing the circulating current. The duty cycle control also provides operation conditions with lower phase-shift values, which decrease the reactive power flow and improves the efficiency.

In Fig. 16, the output voltage and its reference signal waveform, and the output current waveform are shown in Port 1. As it was explained before, the reference currents for Port 2 (DG port) and Port 3 (grid port) are randomly determined and

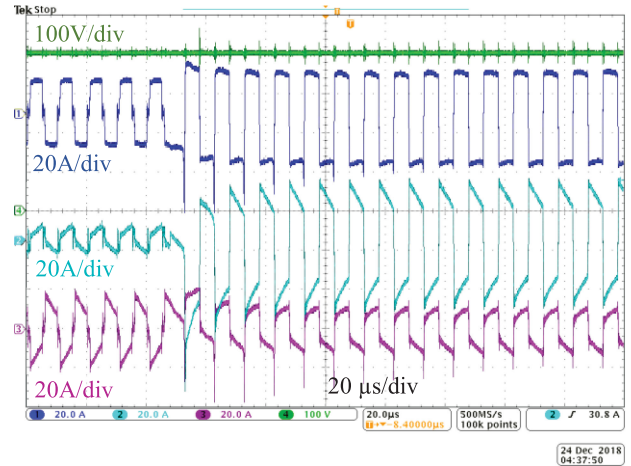


Fig. 17. Port currents and output voltage of the four-port SST at the reference change instant.

some variations are added. The reference current waveform for Port 4 (ESS port) is generated with the PI controller and output voltage error signal. In addition, step load changes are applied and both steady-state and dynamic performance of the proposed control scheme are tested. As it is seen in the figure, the output voltage, Port 2 current and Port 3 current are all tracking their reference signals. The results show that the proposed system is stable and provides fast dynamic response, and the performance of the proposed control scheme is validated. In Fig. 17, currents of the three supply ports (Ch. 1, Ch. 2, and Ch. 3) and the output voltage (Ch. 4) are given at the applied reference variation. The power reference is increased for Port 2 (Ch. 1), increased and reversed for Port 3 (Ch. 2), and decreased and reversed for Port 4 (Ch. 3). It is seen that the proposed four-port SST and duty cycle-based control scheme provide stable operation and fast transient response without any oscillations.

### V. CONCLUSION

In this study, a four-port SST topology, including three active bidirectional converters and one diode bridge unidirectional converter, is introduced. The converter is developed for fast, modular, and isolated utilization of DG/ESS in the power system. The circuitry of the converter is mathematically analyzed, and a two-layer control method is developed for controlling the power flow among the ports of the converter and voltage regulation at the uncontrolled output port. The proposed control combines the phase-shift control method and duty cycle control in order to provide wide range of power flow control and voltage regulation. In order to decouple the power sharing equations of the multiport system, a small signal linearization is applied to the equations. Also, a higher level controller is employed to define the power references for each port based on the status of each power source and the load. The power sharing logic receives the status of the connected components such as SoC of the energy storage, generation capability of the DG and grid connection, and specifies the share of power for each port. The proposed four-port SST is implemented using SiC MOSFET

modules operating at up to 100 kHz frequency. The winding configuration of the four winding transformer is analyzed to achieve the best performance for the transformer. The proposed control method is validated with simulation and experimental results. Both simulation and experimental results show that the proposed system can control the power flow among the ports and the load port voltage independently. It is also shown that the proposed system provides smooth control and power transfer between the ports.

#### APPENDIX

By neglecting the magnetization inductance, the equivalent inductances between the ports can be written as follows:

$$L_{12} = L_{21} = \frac{L_1 L'_3 L'_4 + L_1 L'_2 L'_4 + L_1 L'_2 L'_3 + L'_2 L'_3 L'_4}{L'_3 L'_4} \quad (16)$$

$$L_{13} = L_{31} = \frac{L_1 L'_3 L'_4 + L_1 L'_2 L'_4 + L_1 L'_2 L'_3 + L'_2 L'_3 L'_4}{L'_2 L'_4} \quad (17)$$

$$L_{14} = L_{41} = \frac{L_1 L'_3 L'_4 + L_1 L'_2 L'_4 + L_1 L'_2 L'_3 + L'_2 L'_3 L'_4}{L'_2 L'_3} \quad (18)$$

$$L_{23} = L_{32} = \frac{L_1 L'_3 L'_4 + L_1 L'_2 L'_4 + L_1 L'_2 L'_3 + L'_2 L'_3 L'_4}{L_1 L'_4} \quad (19)$$

$$L_{24} = L_{42} = \frac{L_1 L'_3 L'_4 + L_1 L'_2 L'_4 + L_1 L'_2 L'_3 + L'_2 L'_3 L'_4}{L_1 L'_3} \quad (20)$$

$$L_{34} = L_{43} = \frac{L_1 L'_3 L'_4 + L_1 L'_2 L'_4 + L_1 L'_2 L'_3 + L'_2 L'_3 L'_4}{L_1 L'_2} \quad (21)$$

Then, by using (1) and (4)–(7), power equations for each port can be obtained as follows:

$$P_2 = \frac{V_1 V_{TH21-2}}{2\pi^2 f_s L_{12}} \phi_2 (\pi - \phi_2) - \frac{V_2 V_{TH32-3}}{2\pi^2 f_s L_{23}} (\phi_2 - \phi_3) \times (\pi - \phi_2 + \phi_3) - \frac{V_2 V_{TH42-4}}{2\pi^2 f_s L_{24}} (\phi_2 - \phi_4) (\pi - \phi_2 + \phi_4) \quad (22)$$

$$P_3 = \frac{V_1 V_{TH31-3}}{2\pi^2 f_s L_{13}} \phi_3 (\pi - \phi_3) - \frac{V_2 V_{TH32-3}}{2\pi^2 f_s L_{23}} (\phi_3 - \phi_2) \times (\pi - \phi_3 + \phi_2) - \frac{V_3 V_{TH43-4}}{2\pi^2 f_s L_{34}} (\phi_3 - \phi_4) (\pi - \phi_3 + \phi_4) \quad (23)$$

$$P_4 = \frac{V_1 V_{TH41-4}}{2\pi^2 f_s L_{14}} \phi_4 (\pi - \phi_4) - \frac{V_2 V_{TH42-4}}{2\pi^2 f_s L_{24}} (\phi_4 - \phi_2) \times (\pi - \phi_4 + \phi_2) - \frac{V_3 V_{TH43-4}}{2\pi^2 f_s L_{34}} (\phi_4 - \phi_3) (\pi - \phi_4 + \phi_3) \quad (24)$$

It can be seen from the above equations that the power of each port depends on all of the three phase angles. This makes the control of the system very complicated. To decouple the equations, a small gain ( $x + \Delta x$ ) linearization method is applied to the power equations given in (22)–(24), then power equations have two components  $P_x$  and  $\Delta P_x$  as follows [32]:

$$P_2 + \Delta P_2 = \frac{V_1 V_{TH21-2}}{2\pi^2 f_s L_{12}} (\phi_2 + \Delta\phi_2) (\pi - \phi_2 - \Delta\phi_2) - \frac{V_2 V_{TH32-3}}{2\pi^2 f_s L_{23}} (\phi_2 + \Delta\phi_2 - \phi_3 - \Delta\phi_3) \times (\pi - \phi_2 - \Delta\phi_2 + \phi_3 + \Delta\phi_3) - \frac{V_2 V_{TH42-4}}{2\pi^2 f_s L_{24}} (\phi_2 + \Delta\phi_2 - \phi_4 - \Delta\phi_4) \times (\pi - \phi_2 - \Delta\phi_2 + \phi_4 + \Delta\phi_4) \quad (25)$$

$$P_3 + \Delta P_3 = \frac{V_1 V_{TH31-3}}{2\pi^2 f_s L_{13}} (\phi_3 + \Delta\phi_3) (\pi - \phi_3 - \Delta\phi_3) - \frac{V_2 V_{TH32-3}}{2\pi^2 f_s L_{23}} (\phi_3 + \Delta\phi_3 - \phi_2 - \Delta\phi_2) \times (\pi - \phi_3 - \Delta\phi_3 + \phi_2 + \Delta\phi_2) - \frac{V_3 V_{TH43-4}}{2\pi^2 f_s L_{34}} (\phi_3 + \Delta\phi_3 - \phi_4 - \Delta\phi_4) \times (\pi - \phi_3 - \Delta\phi_3 + \phi_4 + \Delta\phi_4) \quad (26)$$

$$P_4 + \Delta P_4 = \frac{V_1 V_{TH41-4}}{2\pi^2 f_s L_{14}} (\phi_4 + \Delta\phi_4) (\pi - \phi_4 - \Delta\phi_4) - \frac{V_2 V_{TH42-4}}{2\pi^2 f_s L_{24}} (\phi_4 + \Delta\phi_4 - \phi_2 - \Delta\phi_2) \times (\pi - \phi_4 - \Delta\phi_4 + \phi_2 + \Delta\phi_2) - \frac{V_3 V_{TH43-4}}{2\pi^2 f_s L_{34}} (\phi_4 + \Delta\phi_4 - \phi_3 - \Delta\phi_3) \times (\pi - \phi_4 - \Delta\phi_4 + \phi_3 + \Delta\phi_3) \quad (27)$$

Here, the power component  $P_x$  represents the operation point of the converter depending on  $V_x$ ,  $V_y$ ,  $L_{xy}$ ,  $V_x$ ,  $\phi_x$ , and  $\phi_y$ , and  $\Delta P_x$  component represents the power variation depending on the variation on  $\Delta\phi_x$ , and  $\Delta\phi_y$ . This makes  $\Delta\phi_x$  and  $\Delta\phi_y$  perturbation control variables. These perturbation variables can be used in the control loop to control the power flow. Then, power variation components can be written as follows:

$$\Delta P_2 = \frac{V_1 V_{TH21-2}}{2\pi^2 f_s L_{12}} (-2\phi_2 + \pi) \Delta\phi_2 - \frac{V_2 V_{TH32-3}}{2\pi^2 f_s L_{23}} \times (-2\phi_3 + 2\phi_2 + \pi) \Delta\phi_3 + \frac{V_2 V_{TH32-3}}{2\pi^2 f_s L_{23}} \times (-2\phi_3 + 2\phi_2 + \pi) \Delta\phi_2 - \frac{V_2 V_{TH42-4}}{2\pi^2 f_s L_{24}} \times (-2\phi_4 + 2\phi_2 + \pi) \Delta\phi_4 + \frac{V_2 V_{TH42-4}}{2\pi^2 f_s L_{24}} \times (-2\phi_4 + 2\phi_2 + \pi) \Delta\phi_2 \quad (28)$$

$$\begin{aligned} \Delta P_3 = & \frac{V_1 V_{TH3_{1-3}}}{2\pi^2 f_s L_{13}} (-2\phi_3 + \pi) \Delta\phi_3 + \frac{V_2 V_{TH3_{2-3}}}{2\pi^2 f_s L_{23}} \\ & \times (-2\phi_3 + 2\phi_2 + \pi) \Delta\phi_3 - \frac{V_2 V_{TH3_{2-3}}}{2\pi^2 f_s L_{23}} \\ & \times (-2\phi_3 + 2\phi_2 + \pi) \Delta\phi_2 - \frac{V_3 V_{TH4_{3-4}}}{2\pi^2 f_s L_{34}} \\ & \times (-2\phi_4 + 2\phi_3 + \pi) \Delta\phi_4 + \frac{V_3 V_{TH4_{3-4}}}{2\pi^2 f_s L_{34}} \\ & \times (-2\phi_4 + 2\phi_3 + \pi) \Delta\phi_3 \end{aligned} \quad (29)$$

$$\begin{aligned} \Delta P_4 = & \frac{V_1 V_{TH4_{1-4}}}{2\pi^2 f_s L_{14}} (-2\phi_4 + \pi) \Delta\phi_4 + \frac{V_2 V_{TH4_{2-4}}}{2\pi^2 f_s L_{24}} \\ & \times (-2\phi_4 + 2\phi_2 + \pi) \Delta\phi_4 - \frac{V_2 V_{TH4_{2-4}}}{2\pi^2 f_s L_{24}} \\ & \times (-2\phi_4 + 2\phi_2 + \pi) \Delta\phi_2 + \frac{V_3 V_{TH4_{3-4}}}{2\pi^2 f_s L_{34}} \\ & \times (-2\phi_4 + 2\phi_3 + \pi) \Delta\phi_4 - \frac{V_3 V_{TH4_{3-4}}}{2\pi^2 f_s L_{34}} \\ & \times (-2\phi_4 + 2\phi_3 + \pi) \Delta\phi_3. \end{aligned} \quad (30)$$

#### ACKNOWLEDGMENT

This material is based upon work supported by the National Science Foundation under Grant No. 1650470. Any opinions, findings, and conclusions or recommendations expressed in this material are those of the author(s) and do not necessarily reflect the views of the National Science Foundation.

#### REFERENCES

- [1] M. Rashidi, A. Bani-Ahmed, R. Nasiri, A. Mazaheri, and A. Nasiri, "Design and implementation of a multi-winding high frequency transformer for MPSST application," in *Proc. IEEE 6th Int. Conf. Renewable Energy Res. Appl.*, Nov. 5–8, 2017, pp. 491–494.
- [2] R. W. A. A. De Doncker, D. M. Divan, and M. H. Kheraluwala, "A three-phase soft-switched high-power-density DC/DC converter for high-power applications," *IEEE Trans. Ind. Appl.*, vol. 27, no. 1, pp. 63–73, Jan./Feb. 1991.
- [3] X. She, A. Q. Huang, and R. Burgos, "Review of solid-state transformer technologies and their application in power distribution systems," *IEEE J. Emerg. Sel. Topics Power Electron.*, vol. 1, no. 3, pp. 186–198, Sep. 2013.
- [4] H. Qin and J. W. Kimball, "Solid-state transformer architecture using AC-AC dual-active-bridge converter," *IEEE Trans. Ind. Electron.*, vol. 60, no. 9, pp. 3720–3730, Sep. 2013.
- [5] J. L. Brooks, *Solid State Transformer Concept Development*. Port Hueneme, CA, USA: Naval Construction Battalion Center, Naval Mater Command, 1980.
- [6] S. Ozdemir, S. Balci, N. Altin, and I. Sefa, "Design and performance analysis of the three-level isolated DC-DC converter with the nanocrystalline core transformer," *Int. J. Hydrog. Energy*, vol. 42, no. 28, pp. 17801–17812, 2017.
- [7] T. Guillod, F. Krismer, R. Färber, C. M. Franck, and J. W. Kolar, "Protection of MV/LV solid-state transformers in the distribution grid," in *Proc. 41st Annu. Conf. IEEE Ind. Electron. Soc.*, Yokohama, Japan, 2015, pp. 3531–3538.
- [8] M. Rashidi, A. Nasiri, and R. Cuzner, "Application of multi-port solid-state transformers for microgrid-based distribution systems," in *Proc. IEEE Int. Conf. Renewable Energy Res. Appl.*, Birmingham, U.K., 2016, pp. 605–610.
- [9] B. Zhou and T. Littler, "Local storage meet local demand: a technical solution to future power distribution system," *IET Gener. Transmiss. Distrib.*, vol. 10, no. 3, pp. 704–711, 2016.
- [10] Y. Wang, F. Han, L. Yang, R. Xu, and R. Liu, "A three-port bidirectional multi-element resonant converter with decoupled power flow management for hybrid energy storage systems," *IEEE Access*, vol. 6, pp. 61331–61341, Oct. 2018.
- [11] C. Zhao, S. D. Round, and J. W. Kolar, "An isolated three-port bidirectional DC-DC converter with decoupled power flow management," *IEEE Trans. Power Electron.*, vol. 23, no. 5, pp. 2443–2453, Sep. 2008.
- [12] J. Zeng, W. Qiao, and L. Qu, "An isolated three-port bidirectional DC-DC converter for photovoltaic systems with energy storage," *IEEE Trans. Ind. Appl.*, vol. 51, no. 4, pp. 3493–3503, Jul./Aug. 2015.
- [13] C. Gu, Z. Zheng, L. Xu, K. Wang, and Y. Li, "Modeling and control of a multiport power electronic transformer (PET) for electric traction applications," *IEEE Trans. Power Electron.*, vol. 31, no. 2, pp. 915–927, Feb. 2016.
- [14] J. E. Huber and J. W. Kolar, "Solid-state transformers: On the origins and evolution of key concepts" *IEEE Ind. Electron. Mag.*, vol. 10, no. 3, pp. 19–28, 2016.
- [15] C. Gu, Z. Zheng, and Y. Li, "A power electronic transformer (PET) with multiport bidirectional resonant DC-DC converters for electric traction applications," in *Proc. IEEE Transp. Electrification Conf. Expo.*, 2015, pp. 1–6.
- [16] A. Clerici, E. Tironi, and F. Castelli-Dezza, "Multiport converters and ESS on 3-kV DC railway lines: Case study for braking energy savings," *IEEE Trans. Ind. Appl.*, vol. 54, no. 3, pp. 2740–2750, May/Jun. 2018.
- [17] L. Wang, Z. Wang, and H. Li, "Asymmetrical duty cycle control and decoupled power flow design of a three-port bidirectional DC-DC converter for fuel cell vehicle application," *IEEE Trans. Power Electron.*, vol. 27, no. 2, pp. 891–904, Feb. 2012.
- [18] B. Farhangi and H. A. Toliyat, "Modeling and analyzing multiport isolation transformer capacitive components for onboard vehicular power conditioners," *IEEE Trans. Ind. Electron.*, vol. 62, no. 5, pp. 3134–3142, May 2015.
- [19] S. Falcones, R. Ayyanar, and X. Mao, "A DC-DC multiport-converter-based solid-state transformer integrating distributed generation and storage," *IEEE Trans. Power Electron.*, vol. 28, no. 5, pp. 2192–2203, May 2013.
- [20] J. Miao, N. Zhang, C. Kang, J. Wang, Y. Wang, and Q. Xia, "Steady-state power flow model of energy router embedded AC network and its application in optimizing power system operation," *IEEE Trans. Smart Grid*, vol. 9, no. 5, pp. 4828–4837, Sep. 2018.
- [21] Y. Chen, P. Wang, H. Li, and M. Chen, "Power flow control in multi-active-bridge converters: Theories and applications," in *Proc. IEEE Appl. Power Electron. Conf. Expo.*, Anaheim, CA, USA, 2019, pp. 1–8.
- [22] S. Dutta and S. R. S. Bhattacharya, "Integration of multi-terminal DC to DC hub architecture with solid state transformer for renewable energy integration," in *Proc. IEEE Energy Convers. Congr. Expo.*, Denver, CO, USA, 2013, pp. 4793–4800.
- [23] S. Roy, A. De, and S. Bhattacharya, "Multi-port solid state transformer for inter-grid power flow control," in *Proc. Int. Power Electron. Conf.*, Hiroshima, Japan, 2014, pp. 3286–3291.
- [24] D. Liu and H. Li, "A ZVS bi-directional DC-DC converter for multiple energy storage elements," *IEEE Trans. Power Electron.*, vol. 21, no. 5, pp. 1513–1517, Sep. 2006.
- [25] H. Tao, J. L. Duarte, and M. A. M. Hendrix, "Three-port triple-half-bridge bidirectional converter with zero-voltage switching," *IEEE Trans. Power Electron.*, vol. 23, no. 2, pp. 782–792, Mar. 2008.
- [26] X. Liu, Z. Zheng, K. Wang, and Y. Li, "An energy router based on multi-winding high-frequency transformer," in *Proc. IEEE Appl. Power Electron. Conf. Expo.*, Long Beach, CA, USA, 2016, pp. 3317–3321.
- [27] H. Bai and C. Mi, "Eliminate reactive power and increase system efficiency of isolated bidirectional dual-active-bridge DC-DC converters using novel dual-phase-shift control," *IEEE Trans. Power Electron.*, vol. 23, no. 6, pp. 2905–2914, Nov. 2008.
- [28] M. A. Juds *et al.*, "Leakage flux mitigation of laminated ribbon core based transformer for a triple active bridge DC-DC converter," in *Proc. MMM-Intermag Joint Conf.*, Washington, DC, USA, Jan. 14–18, 2019, pp. 65–73.
- [29] S. Tiwari, O.-M. Midtgård, and T. M. Undeland, "SiC MOSFETs for future motor drive applications," in *Proc. 18th Eur. Conf. Power Electron. Appl.*, Karlsruhe, Germany, 2016, pp. 1–10.
- [30] L. Barrios, A. Ursúa, L. Marroyo, and P. Sanchis, "Analytical design methodology for litz-wired high-frequency power transformers," *IEEE Trans. Ind. Electron.*, vol. 62, no. 4, pp. 2103–2113, Apr. 2015.

- [31] H. O. Jimenez, "AC resistance evaluation of foil, round and Litz conductors in magnetic components," M.S. thesis, Dept. Energy Environ., Chalmers Univ., Gothenburg, Sweden, 2013.
- [32] M. Grabarek, M. Parchomiuk and R. Strzelecki, "Conjugated control of triple active bridge converter with common HFT," in *Proc. 11th IEEE Int. Conf. Compat. Power Electron. Power Eng.*, Apr. 4–6, 2017, pp. 304–307.



**Mohammad Rashidi** was born in Parsian, Iran, in 1986. He received the B.S. and M.S. degrees from the Amirkabir University of Technology (Tehran Polytechnic), Tehran, Iran, in 2009 and 2012, respectively, and the Ph.D. degree from the University of Wisconsin-Milwaukee, Milwaukee, WI, USA, in 2017, all in electrical engineering power.

He is currently a Lead Power Conversion Engineer with Eaton Research Labs, Eaton Corporation, Menomonee Falls, WI. He is also serving as Chapter Chair of IEEE PES chapter at Milwaukee section. He

has authored or coauthored more than four conference and journal papers. His current research interests include modeling and assessing of microgrids, and design and implementation of power electronic converters for grid-connected distributed energy resources.



**Necmi N. Altin** (M'11–SM'19) received the B.Sc., M.Sc., and Ph.D. degrees from Gazi University, Ankara, Turkey, in 2000, 2003, and 2009, respectively.

He joined the Department of Electrical and Electronics Engineering, Faculty of Technology, Gazi University, as an Assistant Professor in 2010, and was promoted to an Associate Professor position in 2014. He has been a Visiting Scholar with the University of Wisconsin-Milwaukee, USA, from 2017 to 2019. His current research interests include power electronics,

application of power electronics in renewable energy systems, high power factor rectifiers, grid interactive inverters, solid-state transformers, and control systems.

Dr. Altin is currently serving as an Associate Editor for the IEEE TRANSACTIONS ON INDUSTRY APPLICATIONS for Renewable and Sustainable Energy Conversion Systems Committee.



**Saban S. Ozdemir** (S'12–M'14) received the B.Sc., M.Sc., and Ph.D. degrees in electrical education from Gazi University, Ankara, Turkey, in 2004, 2007, and 2013, respectively.

From 2008 to 2009, he was with Baskent University, Ankara. In 2009, he joined Gazi University. He is currently an Associate Professor with the Department of Energy System Engineering, Faculty of Technology, Gazi University. He was a Visiting Scholar with the University of Wisconsin-Milwaukee from 2017 to 2019. His current research interests include power

electronics, uninterruptible power supplies, grid interactive inverters, power quality, and solid-state transformers.

Dr. Ozdemir is currently serving as an Associate Editor for the IEEE TRANSACTIONS ON INDUSTRY APPLICATIONS for Renewable and Sustainable Energy Conversion Systems Committee.



**Abedalsalam Bani-Ahmed** (M'11) was born in Sakib, Jordan. He received the B.Sc. degree in engineering technology from Yarmouk University, Irbid, Jordan, in 2007, the M.Sc. degree in computer engineering from the Jordan University of Science & Technology, Irbid, in 2011, and the Ph.D. degree in electrical engineering from the University of Wisconsin-Milwaukee (UW-Milwaukee), Milwaukee, WI, USA, in 2017, specializing in the cyber-physical integration in decentralized smart microgrid control systems.

He was a Research Assistant with the Center for Sustainable Electrical Energy Systems (UW-Milwaukee) from 2012 to 2017, and a Power Systems Engineer with Eaton Corporation in 2017. He is currently a Specialist in power systems cybersecurity and resiliency with Eaton Corporation Research Labs, Menomonee Falls, WI, USA. He has authored or coauthored numerous technical journal and conference papers, and white papers-related topics. His research interests include smart grids, microgrids, and distributed energy resource management system (DERMS), industrial Internet of Things (IIoT) communications infrastructure, protocols, cybersecurity, and standards.

Dr. Bani-Ahmed is currently serving in IEEE Smart Grid R&D, Operations committees, IEEE Smart Cities R&D, Education, and Publication committees. He also serves as a Reviewer to multiple IEEE Power & Energy Society (PES) and Industry Applications Society (IAS) transactions, and various international smart grid-related journals. He is an active member in the following societies: IEEE PES, IEEE Computer Society, IEEE IAS, and IEEE Communications Society.



**Adel Nasiri** (SM'06) received the B.S. and M.S. degrees from the Sharif University of Technology, Tehran, Iran, in 1996 and 1998, respectively, and the Ph.D. degree from the Illinois Institute of Technology, Chicago, IL, USA, in 2004, all in electrical engineering.

He was with Moshanir Power Engineering Company from 1998 to 2001. He was also with ForHealth Technologies, Inc., Daytona Beach, FL, from 2004 to 2005. He is currently a Professor and the Director of the Center for Sustainable Electrical Energy Sys-

tems, College of Engineering and Applied Sciences, University of Wisconsin-Milwaukee. He is a Co-Author of the book *Uninterruptible Power Supplies and Active Filters* (Boca Raton, FL, USA: CRC Press). His research interests include renewable energy interface, energy storage, and microgrids. He has authored or coauthored numerous technical journal and conference papers on related topics. He also has seven patent disclosures.

Dr. Nasiri is currently the Paper Review Chair for IEEE TRANSACTIONS ON INDUSTRY APPLICATIONS, an Editor of *Power Components and Systems*, and an Associate Editor for the *International Journal of Power Electronics*, and was an Editor for IEEE TRANSACTIONS ON SMART GRID (2013–2019). He was the General Chair of 2012 IEEE Symposium on Sensorless Electric Drives, 2014 International Conference on Renewable Energy Research and Applications, and 2014 IEEE Power Electronics and Machines for Wind and Water Applications.